Histochem Cell Biol (2014) 142:171–184
DOI 10.1007/s00418-014-1189-y

ORIGINAL PAPER

Electron tomography and cryo-SEM characterization reveals novel ultrastructural features of host-parasite interaction during *Chlamydia abortus* infection

M. Wilkat · E. Herdoiza · V. Forsbach-Birk · P. Walther · A. Essig

Accepted: 22 January 2014 / Published online: 13 February 2014

Abstract *Chlamydia* (*C*.) *abortus* is a widely spread pathogen among ruminants that can be transmitted to women during pregnancy leading to severe systemic infection with consecutive abortion. As a member of the *Chlamydiaceae*, *C*. *abortus* shares the characteristic feature of an obligate intracellular biphasic developmental cycle with two morphological forms including elementary bodies (EBs) and reticulate bodies (RBs). In contrast to other chlamydial species, *C*. *abortus* ultrastructure has not been investigated yet. To do so, samples were fixed by high-pressure freezing and processed by different electron microscopic methods. Freeze-substituted samples were analysed by transmission electron microscopy, scanning transmission electron microscopical tomography and immuno-electron microscopy, and freeze-fractured samples were analysed by cryo-scanning electron microscopy. Here, we present three ultrastructural features of *C*. *abortus* that have not been reported up to now. Firstly, the morphological evidence that *C*. *abortus* is equipped with the type three secretion system. Secondly, the accumulation and even coating of whole inclusion bodies by membrane complexes consisting of multiple closely adjacent membranes which seems to be a *C*. *abortus* specific feature. Thirdly, the formation of small vesicles in the periplasmic space of RBs in the second half of the developmental cycle. Concerning the time point of their formation and the fact that they harbour chlamydial components, these vesicles might be morphological correlates of an intermediate step during the process of redifferentiation of RBs into EBs. As this feature has also been shown for *C*. *trachomatis* and *C*. *pneumoniae*, it might be a common characteristic of the family of *Chlamydiaceae*.

Keywords *Chlamydia abortus* · Transmission electron microscopy · STEM tomography · Developmental cycle · High-pressure freezing

M. Wilkat (✉) · V. Forsbach-Birk · A. Essig
Institute of Medical Microbiology and Hygiene, University Hospital of Ulm, Albert-Einstein-Allee 23, 89081 Ulm, Germany
e-mail: max.wilkat@uni-ulm.de

E. Herdoiza · P. Walther
Central Facility for Electron Microscopy, Ulm University, Albert-Einstein-Allee 11, 89069 Ulm, Germany

Introduction

The *Chlamydiaceae* family comprise obligate intracellular replicating human and animal pathogens which are of considerable clinical and epidemiological importance worldwide. Prominent members are *Chlamydia* (C.) *trachomatis*, *C*. *pneumoniae*, *C*. *psittaci* and *C*. *abortus*. *C*. *trachomatis* causes oculogenital infection, including blinding trachoma, lymphogranuloma venereum and non-gonococcal urethritis and cervicitis. *C*. *pneumoniae* causes infections of the upper and lower respiratory tract, and *C*. *psittaci* is the causative agent of ornithosis, a severe pneumonia that can be transmitted from birds to humans. *C*. *abortus* is associated with ruminant abortion and has been broadly detected in sheep, goats and calves causing considerable economic damage in the agriculture worldwide (Longbottom and Coulter 2003). As a zoonotic pathogen, it can be transmitted to pregnant women posing a life-threatening health risk. If not treated appropriately, the patients may develop severe septicaemia with disseminated intravascular coagulation resulting in spontaneous abortion of the child (Baud et al. 2008; Walder et al. 2005).

All members of the *Chlamydiaceae* share a biphasic developmental cycle involving infectious, spore-like elementary bodies (EB: about 300 nm in diameter) and

metabolically active reticulate bodies (RB: about 1 μm in diameter), which divide within a non-fusogenic inclusion. This distinct developmental cycle is known for over 80 years, since the first description by Bedson and Bland (1932). However, the molecular details of the host–pathogen interaction including cell entry, intracellular differentiation and release are poorly understood.

Electron microscopy observations in the 1970s and 1980s revealed new ultra morphological features: Matsumoto et al. described 'surface projections' and 'B-structures' on RBs and EBs of *C. psittaci* (Matsumoto and Manire 1970; Matsumoto 1982a, b). The *Chlamydia* type III secretion system (T3SS) has been identified as a molecular syringe-like structure behind these surface projections. It enables chlamydiae to secret effector proteins into the host cell, which is considered nowadays to be a central mechanism of chlamydial virulence being essential for the intracellular survival (Betts-Hampikian and Fields 2010; Peters et al. 2007). Until the genetic proof in 1997 for the existence of the T3SS in chlamydiae (Hsia et al. 1997), the morphological observations of these surface projections were the first and only hints that chlamydiae are equipped with a T3SS.

In general, studies systematically investigating ultrastructural features and species specific differences are rare. Chi et al. (1987) demonstrated that EBs of *C. pneumoniae* in contrast to *C. trachomatis* and *C. psittaci* show a 'pear-shaped' outer membrane with a pointed end. This distinct morphological difference has been proposed to lead to a different process of attachment to and endocytosis by the host cell (Kuo et al. 1988).

In this report, we describe ultrastructural features of *C. abortus* strain S26/3 along the developmental cycle in experimentally infected HeLa229 and McCoy cells in comparison with *C. trachomatis* and *C. pneumoniae*.

Materials and methods

Organisms and cultivation

The strains *C. abortus* S26/3 (Thomson et al. 2005), *C. trachomatis* (serovar D strain UW-3/Cx, American Type Culture Collection: VR-885) and *C. pneumoniae* (TWAR strain TW-183, ATCC: VR-2282) were used for the study and cultivated on HeLa229 cell monolayers (ATCC: CCL-2.1) or McCoy cell monolayers (ATCC: CRL-1696) in Quantum 101 (PAA Laboratories, Pasching, Austria) according to standard procedures.

Sapphire discs (3 mm diameter, thickness about 50 μm; Brügger, Minusio, Switzerland, distributed by Engineering Office M. Wohlwend GmbH, Sennwald, Switzerland) were cleaned in sulphuric acid, soapwater and absolute ethanol and subsequently coated with 20 nm of carbon by electron beam evaporation with a BAF 300 (BAL-TEC, Balzers, Principality of Liechtenstein). After UV irradiation, sapphire discs were placed into the cavities of a 12-well culture plate and HeLa229 cells or McCoy cells were seeded in the culture plate wells to obtain confluent cell monolayers on sapphire discs. Cell monolayers were experimentally infected with *C. abortus*, *C. trachomatis* and *C. pneumoniae*, respectively, at a multiplicity of infection of five.

High-pressure freezing (HPF)

Sample preparation for electron microscopy was carried out as described (Walther et al. 2013) with some modification. Sapphire discs containing infected cells were high-pressure frozen without any chemical pre-fixation at different points after infection (6 or 8 h intervals, depending on chlamydial species) using the Wohlwend HPF Compact 01 (Engineering Office M. Wohlwend GmbH, Sennwald, Switzerland). The sapphire discs were clamped between two aluminium planchettes (diameter 3 mm). One planchette was flat, and the other had a central cavity of 100 μm in depth and 2 mm in diameter. The cavities between the tissue and the aluminium planchettes were filled with hexadecene (Studer et al. 1989). Hexadecene is not miscible with water and does not serve as a cryo-protectant, but helps to transfer the pressure and temperature during HPF. The frozen samples were stored in liquid nitrogen until freeze-substitution was performed.

Freeze-substitution and embedding

The high-pressure frozen samples were carefully removed from the aluminium planchettes in liquid nitrogen and immersed in 1 mL freeze-substitution medium pre-cooled to −90 °C. The freeze-substitution media consisted of acetone (VWR International GmbH, Darmstadt, Germany) with 0.2 % osmium tetroxide (Merck KGaA, Darmstadt, Germany), 0.1 % uranyl acetate (Merck KGaA, Darmstadt, Germany) and 5 % of water for good membrane contrast (Buser and Walther 2008). We used a specially designed computer-controlled substitution apparatus (A. Ziegler and W. Fritz, Central Facility for Electron Microscopy, Ulm University, unpublished data) to slowly warm the samples from −90 to 0 °C over a period of 16 h in an exponential warming protocol. The samples were kept at room temperature for 30 min, washed with the respective solvent and embedded in a two-step Epon series (Fluka) of 50 % Epon in solvent for 1 h, 100 % Epon for 6 h. The Epon was then polymerized for 48 h at 60 °C, and 60-nm-thin sections were cut with a Leica Ultracut UCT ultra-microtome using a diamond knife (Diatome, Biel, Switzerland), collected on bare copper grids. Section staining with lead citrate was performed.

For immuno-electron microscopy, the freeze-substitution medium did not contain osmium tetroxide and low-temperature embedding was performed to better conserve antigenicity. So, the freeze-substitution medium consisted of acetone (VWR International GmbH, Darmstadt, Germany) with 0.1 % uranyl acetate (Merck KGaA, Darmstadt, Germany) and 5 % of water. For low-temperature embedding, LR-Gold samples were substituted from −90 to −20 °C for 16 h, washed twice with pre-cooled acetone, infiltrated for 2 h with 50 % (v/v) LR-Gold in acetone and for 1 h with 100 % LR-Gold. The polymerization was carried out at −18 °C over night under an UV-lamp. LR-Gold always contained 0.1 % (w/w) benzil and 0.1 % (w/w) benzoyl peroxide. Sections were cut as described above, collected on carbon-formvar-coated copper grids and marked with different gold-coupled antibodies as described below.

Transmission electron microscopy (TEM)

The ultra-thin sections were imaged with a JEM-1400 transmission electron microscope (Jeol GmbH, Eching, Germany) at an acceleration voltage of 120 kV. The images were recorded with a Veleta digital camera (Olympus Soft Imaging Solutions GmbH, Münster, Germany) with a resolution of 2,024 × 2,024 pixel and the iTEM software (Olympus Soft Imaging Solutions GmbH, Münster, Germany). No additional image processing apart from brightness/contrast correction and insertion of marks was performed. Multiple sections of at least two independent samples were compared for their structural quality.

Scanning transmission electron microscopical tomography (STEM tomography)

For STEM tomography, semi-thin sections of 500 nm thickness were collected on bare copper grids with parallel grid bars in one direction only. To attach the relatively thick sections on the grid bars, the copper grids were coated with poly-L-lysine (10 % in water) before the sections were attached. The grids were then warmed on a heating table to a temperature of 60 °C to flatten the sections. Afterwards, the sections were again coated with poly-L-lysine to attach on both sample sides the 15-nm colloidal gold particles (Aurion, The Netherlands), serving as fiducial markers for the calculation of the tomograms. Finally, the mounted sections were carefully coated with 5 nm carbon from both sides by electron beam evaporation to increase electrical conductivity and mechanical stability. Before imaging, the samples were plasma-cleaned for 10 s.

Tilt series were recorded with a TITAN microscope (FEI) at 300 kV in scanning transmission mode (STEM) from ±70° in 1° steps and reconstructed using the IMOD software (Kremer et al. 1996) (Boulder Laboratory for 3-D Electron Microscopy of Cells, Boulder, USA) as described by Höhn et al. (2011). For segmentation and data display, the AMIRA software (Visage Imaging GmbH, Berlin, Germany) was used.

Immuno-electron microscopy

Ultrathin sections were incubated in 4 % goat serum in PBS (phosphate-buffered saline, pH 7.6) and incubated with monoclonal mouse-antibodies against chlamydial heat shock Protein 60 (HSP60) (Dianova GmbH, Hamburg, Germany) and chlamydial lipopolysaccharide (LPS) (kindly provided by H. Brade, Forschungszentrum Borstel, Germany) (Fu et al. 1992). After thoroughly washing with PBS, incubation with the second antibody (goat antimouse coupled to 10 nm gold particles, Aurion, Wangeningen, The Netherlands) followed (Roth et al. 1996). The sections were post-fixed with glutaraldehyde and post-stained with uranylacetate. TEM was performed as described above.

Freeze-fracturing and cryo-scanning electron microscopy (cryo-SEM)

For freeze-fracturing, 170-μm-thick sapphire discs have been used as described by Walther et al. (2013). Cells were grown on these discs and infected. The samples were chemically prefixed at 64 h post-infection (p.i.) with 2 % glutaraldehyde. A 50-μm-thick gold spacer ring (diameter 3.05 mm, central bore 2 mm; Plano GmbH, Wetzlar, Germany) was mounted between two 170-μm-thick sapphire discs with the infected cells facing each other. These sandwiches were high-pressure frozen without aluminium planchettes and without the use of hexadecene.

The frozen sandwiches (either sapphire or aluminium) were mounted on a Bastacky holder (Walther 2003). After transfer to the BAF 300 freeze-etching device (Bal-Tec, Principality of Liechtenstein), the temperature of the sample stage was raised to 155 K (vacuum about 2×10^{-7} mbar). The sandwiches were cracked with a steel knife and then double-layer coated as described by Walther et al. (1995) by electron beam evaporation with 3 nm of platinum–carbon from an angle of 45° and perpendicularly with about 6 nm of carbon. Thereby, the additional carbon coat increases electrical conductivity (prevents charging) and, even more importantly, reduces the effects of beam damage.

The specimens were imaged with a S-5200 ultra-high resolution field emission scanning electron microscopy (Hitachi High Technologies America, Schaumburg, USA) at an acceleration voltage of 10 kV using the backscattered electron signal (Walther et al. 1995). No additional image processing apart from brightness/contrast correction and insertion of marks was performed.

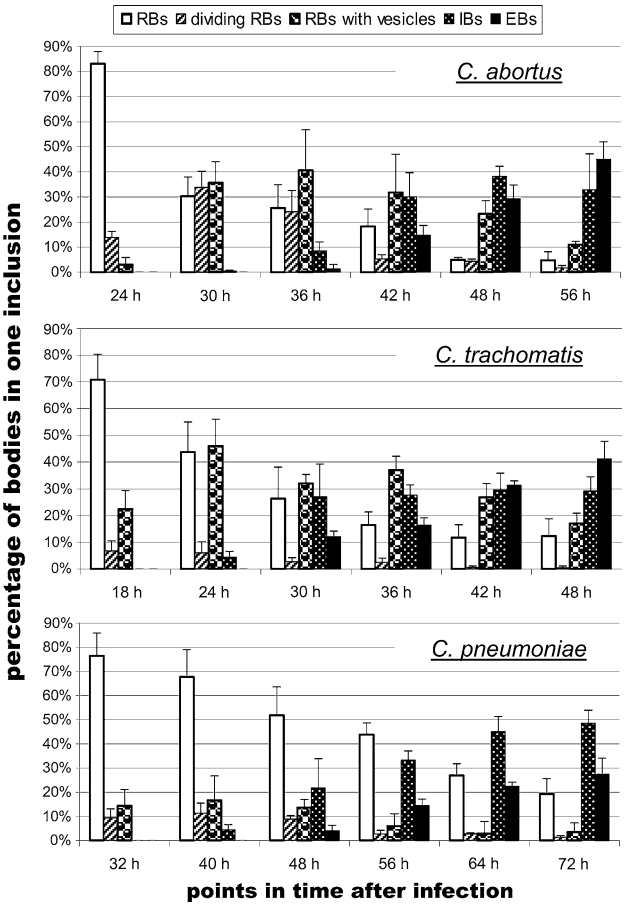

Fig. 1 Relative amount of different morphological forms of chlamydiae inside the inclusion of one infected HeLa229 cell during the second half of the developmental cycle for each point in time after infection and each chlamydial species. The duration of the developmental cycle for each species was set due to the ratio of RBs to EBs. TEM samples of HeLa229 cells infected with each chlamydial species, respectively, were evaluated. For each point in time after infection, the entirety of morphological forms of the inclusions of seven host cells visible in thin sections based on two independent infection experiments was counted (300–8,000 organisms per sample depending on the point of time after infection). The height of a *bar* shows the arithmetic average of the relative amount, and the *error bar* indicates the standard deviation

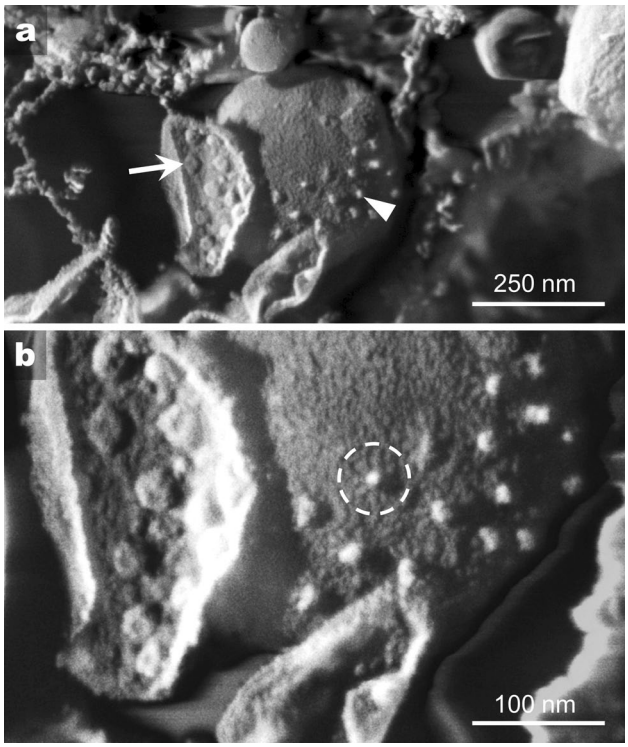

Fig. 2 Projections and B-structures upon the surface of EBs inside an inclusion as observed by cryo-SEM of a freeze-fracture sample of *C. abortus* infected HeLa229 cells 64 h p.i. **a** The true surface of an EB is shown. *White arrowhead* points towards projections on the outer membrane of an EB. *White arrow* indicates the concave face of an outer membrane of a chlamydial body revealing the button structures (B-structures). *Bar* 250 nm. **b** A larger scale of magnification: each projection is arising from the centre of a flower-like structure consisting of several leaves (example marked by a *circle*), and each B-structure shows a cavity in its centre. *Bar* 100 nm

Statistic evaluation

To determine the amount of different morphological forms of intracellular chlamydiae, the inclusion of seven cells visible in thin sections based on two independent infection experiments was analysed for each point in time after infection. RBs, dividing RBs, RBs with vesicles in the periplasmic space, intermediate body (IBs) and EBs were distinguished. The total number of counted organisms was about 300 at early time points and up to 8,000 at late time points. The relative frequency of one type of morphological form is expressed as the arithmetic average for each point in time after infection. The size of the measured objects was calculated as the average of the two largest perpendicular diameters.

Results

The systematic analysis of the ultrastructure of *C. abortus* during its entire developmental cycle showed that it shares the known main features of the *Chlamydiaceae*, involving the uptake of EBs by the host cell, the intracellular maturation and division of RBs, the condensation of RBs to EBs and finally the release of EBs into the host cell's environment. The duration of the developmental cycle of *C. abortus* was set between *C. trachomatis* (ca. 48 h) and *C. pneumoniae* (ca. 72 h) and took about 56 h (Fig. 1).

Strikingly, three noteworthy features occurred which have not been reported yet and are presented in detail in the following.

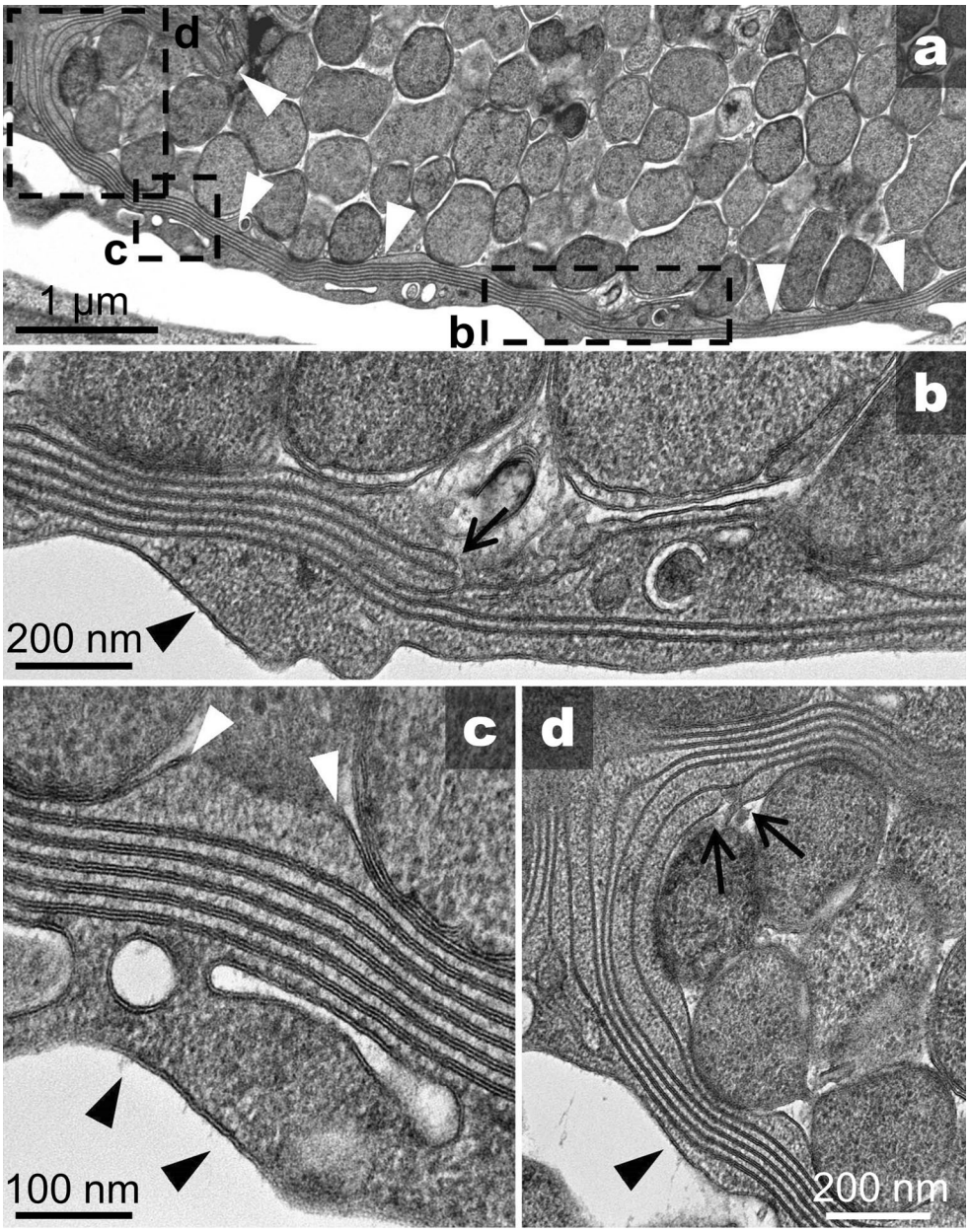

Fig. 3 Lamelliform inclusion membrane complex running like rails all around the inclusion as seen by TEM of a thin section of *C. abortus* infected HeLa229 cells 30 h p.i. **a** Overview: *white arrowheads* point towards the inclusion membrane (also in **c**). *Bar* 1 µm, details in *b*, *c*, *d*. **b** *Black arrow* shows the switching point of the membrane (also in **d**), where it runs into the opposite direction thereby bordering a blind-ending tube. *Black arrowhead* points to the plasma membrane of the host cell (also in **c** and **d**). *Bar* 200 nm. **c** 10 membranes run parallel to each other around the inclusion. *Bar* 200 nm. **d** Inclusion membranes run around the inclusion pole. *Bar* 200 nm

The outer membrane of *C. abortus* exposed surface projections and B-structures

Cryo-SEM images of freeze-fracture samples of *C. abortus* infected cells were analysed for the presence of ultrastructural correlates of the T3SS. Typical structures were basically identified on the surfaces of EBs at a late stage of the developmental cycle. These morphological correlates of the T3SS could only be found on approximately 10 % of EBs per inclusion. A SEM image showing ultra-structures on the surface of an EB (350 nm in diameter) being representative for the T3SS is illustrated in Fig. 2. The true surface of an EBs outer membrane showed 10–20 projections each arising from the centre of a flower-like structure. This structure measured 36 nm in diameter and consisted of 8–10 radial arrayed leaves. The inner concave face of an EBs outer membrane revealed 10–20 button structures (B-structures). These B-structures measured 30 nm in

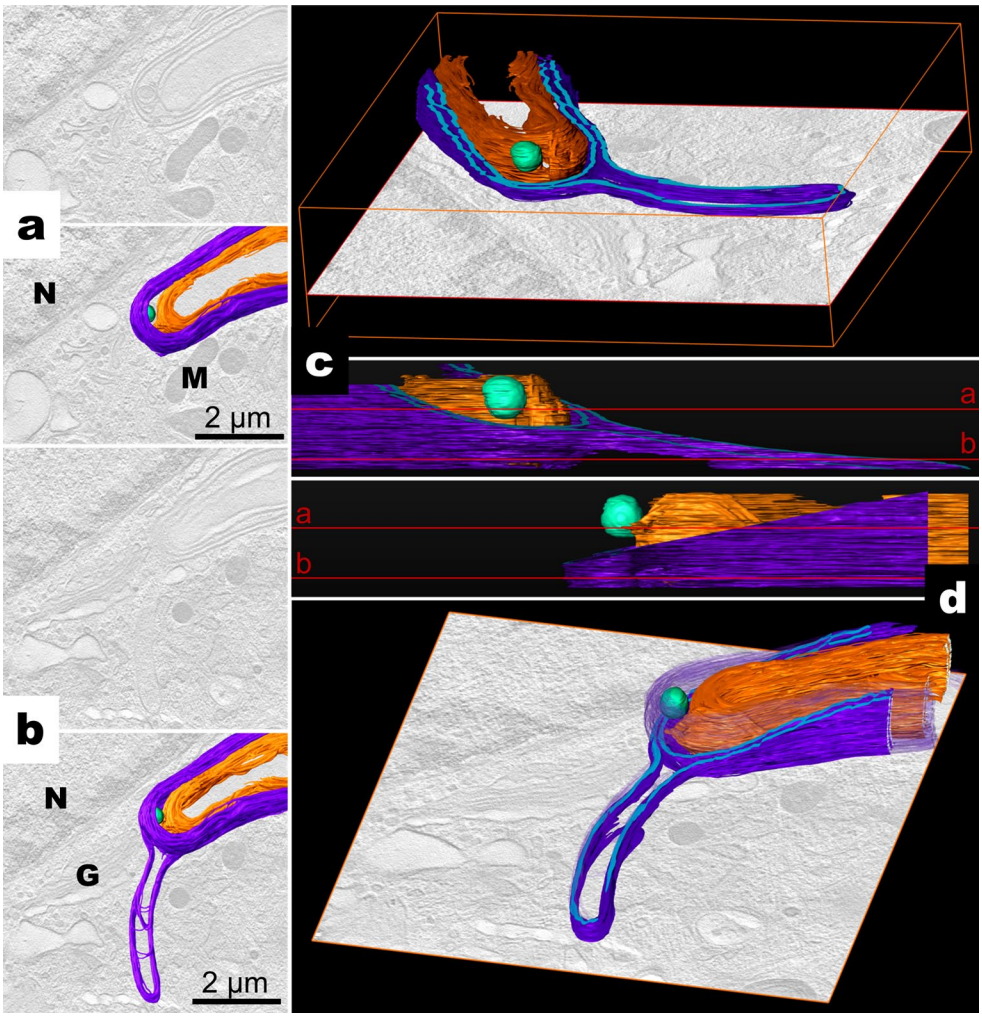

Fig. 4 Three-dimensional intricacy of the *C. abortus* membrane complexes inside infected HeLa229 cells 30 h p.i. as revealed by STEM tomography and 3D-reconstruction. An inner pair of membranes (*orange*) runs parallel to an outer, encoating pair (*purple*) which has an extension of 4 µm. In between those membranes, there is a further membrane vesicle (*green*). The compartments between the different membranes show an electron density similar to the cytoplasm and a lesser electron density in an alternating pattern. **a**, **b** Two sections (section level shown in **c**, **d**) of the calculated volume with and without reconstruction show that those two membrane pairs (*orange*, *purple*) merge at some section levels. *N* host cell's nucleus, *M* mitochondria, *G* golgi, *bar* 2 µm. **c**, **d** The three-dimensional reconstruct of the membrane complex from different perspectives. The *purple* pair of membranes is cut along the *blue* line to reveal the view upon the *orange* pair of membranes and their discreet merging point

diameter and had a central cavity of about 8 nm in diameter. Both the projections on the outer convex surface and the B-structures on the inner concave surface were hexagonally arrayed and could only be found in a limited area of an EBs outer membrane surface. The centre-to-centre spacing between the different projections or B-structures was about 52 nm, respectively.

Membrane complexes associated with the *C. abortus* inclusion occurred in the second half of the developmental cycle

A remarkable feature of the *C. abortus* developmental cycle could be observed from 24 h p.i. onwards: the formation of massive membrane complexes inside the host cell's cytoplasm in close association with the inclusion (Fig. 3). In thin sections, more than 70 % of the infected host cells exhibited these membrane complexes. They consisted of tubes bordered by a single bi-layered membrane. The inside of those tubes showed a similar electron density as the host cell's cytoplasm. Their thickness varied from 30 to 150 nm depending on the surrounding space. In some samples, the tubes were pushed closely together in stacks so that their bordering membranes added up to a pattern as shown in Fig. 3c: long rails of pairs of membranes running around one pole of an inclusion. These closely adjacent membranes resemble to the inner and outer membrane of an active mitochondrion, the only organelle having such closely related membranes. Sometimes, a single membrane of one tube made a u-turn thereby bordering a blind end of the tube (Fig. 3b, d). In the three-dimensional reconstruction of a membrane complex, these tubes exhibited such a height that they seem to be rather membrane walls (Fig. 4). The spacial build-up of these walls to a membrane complex was intricate; at some section levels, they appeared to be encased like onion skins or simply lying upon another in stacks. The number of complex-forming membrane tubes varied between 2 and 12. The dimension of the membrane complexes inside the host cell was up to 12 µm depending on the point in time after infection.

The subcellular localization of the membrane complexes was strongly associated with the inclusion. In more than

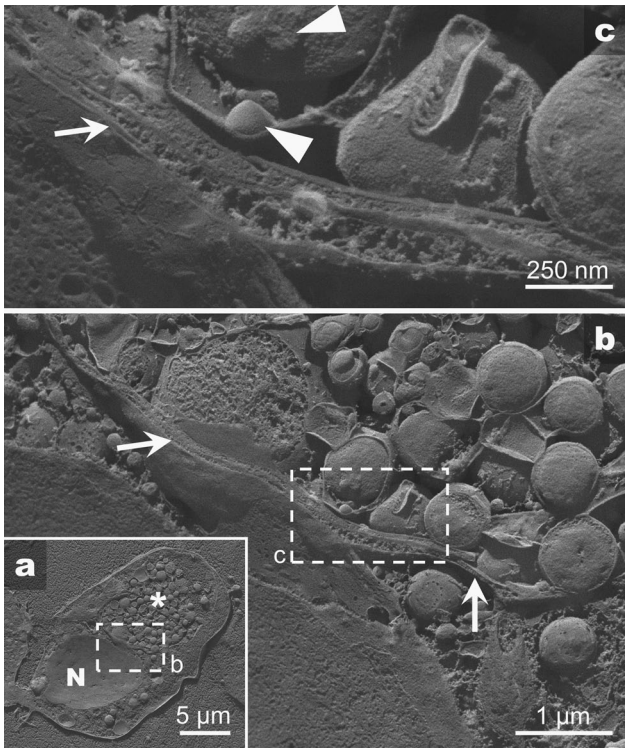

Fig. 5 SEM images of freeze-fracture samples showing the inclusion membrane complex and RBs inside the inclusion of a *C. abortus* infected HeLa229 cell 64 h p.i. **a** Overview, *N* host cell's nucleus, *asterisk* inclusion, *bar* 5 µm, detail in *b*. **b** *White arrows* point to the inclusion membrane, which shows its *C. abortus* specific lamelliform structure consisting of more than just one membrane running around the inclusion. *Bar* 1 µm, detail in *c*. **c** Near the inclusion membrane, there is an RB with a fractured outer membrane revealing its periplasmic space, and *white arrowhead* points towards a vesicle inside the periplasmic space and towards a protuberance of the RB's main body which is possibly a budding vesicle. *Bar* 250 nm

90 % of the membrane complex exhibiting cells, it seemed that the inclusion membrane itself had been twisted around forming the complex. This inclusion membrane complex was not found around the entire inclusion's circumference, but exhibited around the nucleus-orientated pole of the inclusion or, in case of multiple inclusions in one host cell, between multiple inclusions (Figs. 5, 7). In less than 10 % of the infected cells membrane complexes were found somewhere in the host cell's cytoplasm without any association with the inclusion. Neither in *C. trachomatis* nor in *C. pneumoniae* infected cell cultures, membrane complexes could be found (data not shown).

Further observations on the distribution of host mitochondria inside *C. abortus* infected host cells revealed strong mitochondrial association with the inclusion and the inclusion membrane complex (Figs. 6, 7). From the middle-to-late stages, mitochondria were found huddling against the inclusion membrane with a minimal spacing of 4 nm. The ultrastructure of these mitochondria associated with the inclusion membrane changed during the late stages of the developmental cycle. The typical cristae structure was fading. Instead, structures consisting of electron-dense vesicles bordered by one outer membrane occurred at late stages of the developmental cycle (Fig. 7c, d). These structures gave the impression of perishing mitochondria.

Chlamydia abortus showed periplasmic vesicles during the late stages of the developmental cycle

Chlamydia abortus inclusions are shown at 24 h p.i. and 42 h p.i. (Fig. 7). The ultrastructure of RBs inside the inclusion changed during the developmental cycle. Up to 24 h p.i., RBs' inner and outer membrane lay to one another whereby the periplasmic space measured 20 nm at most or was hardly discernible in TEM sections. At 24 h p.i., the periplasmic space began to widen starting at one side of an RB. From this time on to the late stages of the developmental cycle, vesicles in the periplasmic space of RBs occurred in every infected host cell (Figs. 7b–d, 8, also in Figs. 5c, 6b, d). Their number varied from 1 to 15 depending on the point of time after infection. These vesicles showed a spherical to tubular shape and measured about 62 ± 23 nm (mean ± standard deviation) in diameter (average of 200 vesicles). Their inside had the same electron density as the main body. They were bordered by a single bi-layered membrane. Some RBs showed vesicular protuberances of the same size as the vesicles, possibly being the morphological correlate to the process of vesicles either fusing with or budding off the main body. Immuno gold-labelling of chlamydial LPS and HSP60 (Fig. 8c, d) indicated that these chlamydial components were found inside the vesicles suggesting that budding off was the more probable process behind the protuberances. Figure 9 gives an idea of the three-dimensional morphology of RBs with vesicles in the periplasmic space underlining the spherical to tuberal shape of vesicles and the fact of protuberances being vesicles still connected to the main body. The outer membrane encased the main body and the vesicles without any discontinuity.

The number of *C. abortus* RBs with vesicles in the periplasmic space started to increase from 24 h p.i. and reached its maximum at 36 h p.i. with a relative amount of 41 % (Fig. 1). In this time span, the number of normally shaped RBs constantly decreased. From 36 h p.i. onwards, the number of RBs with vesicles in the periplasmic space decreased, while the IBs and EBs began to increase. Due to the asynchronous maturation of chlamydial bodies (compare Figs. 6a, 7b, both 42 h p.i.), the standard deviation of the relative amount of differently shaped bodies in one inclusion (indicated as error bars in Fig. 1) was relatively big. However, the dynamic of this sequence of different chlamydial morphologies over the time suggested that RBs

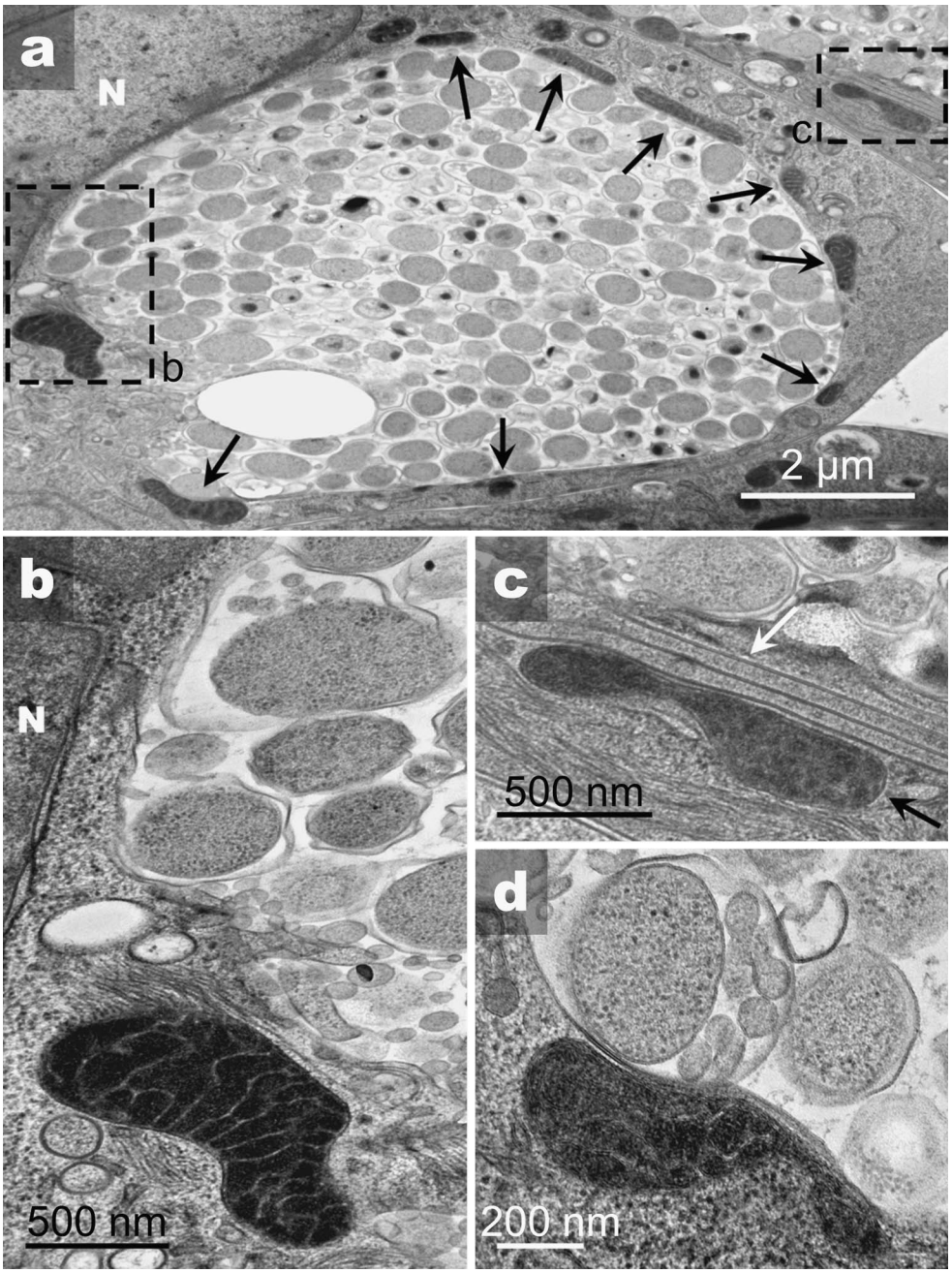

Fig. 6 Relation between mitochondria and the *C. abortus* inclusion inside infected HeLa229 cells 42 h p.i. as observed by TEM. **a** *Black arrows* point towards mitochondria next to the inclusion huddling against the inclusion membrane. Inside the inclusion, there are RBs, RBs with vesicles in the periplasmic space, IBs and EBs. *N* host cell's nucleus, *bar* 2 µm, details in *b*, *c*. **b**, **c** A mitochondrion (*b*) next to the inclusion showing its christae which seem to fall apart forming small vesicles, just like a much less healthier mitochondrion in the neighbouring cell (*c*). *White arrow* points towards a membrane complex around the *C. abortus* inclusion. *Bar* 500 nm. **d** Another unhealthy looking mitochondrion next to an inclusion harbouring RBs with vesicles inside the periplasmic space. *Bar* 200 nm

with vesicles in the periplasmic space might be an intermediate step during the redifferentiation process of RBs to EBs.

The formation of vesicles in the periplasmic space could also be observed in *C. trachomatis* and *C. pneumoniae* (Fig. 8e, f). *C. trachomatis* showed slightly smaller vesicles than *C. abortus* and *C. pneumoniae*, and they measured 55 ± 16 nm (average of 200 vesicles). Strikingly, in *C. abortus* and *C. trachomatis*, the widened periplasmic space harbouring the vesicles was located like a crescent at one side of an RB or was massively widened, whereas the periplasmic space of *C. pneumoniae* was predominantly

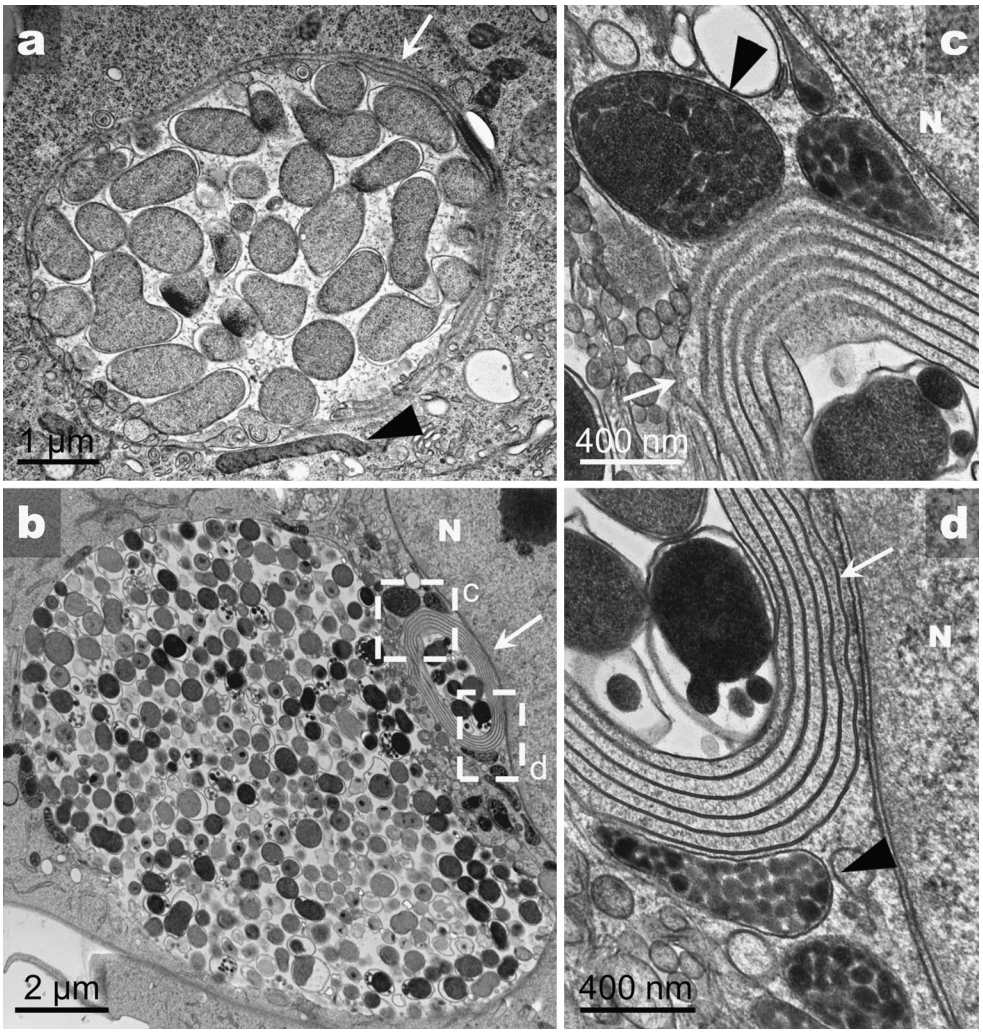

Fig. 7 *Chlamydia abortus* inclusions at 24 and 48 h p.i. showing the differences between the proliferation and the terminal phase of the *C. abortus* developmental cycle inside HeLa229 cells as seen by TEM **a** 24 h p.i.: RBs proliferating inside the yet small (5 µm in diameter) inclusion. Their periplasmic space is broadened at one side of the RB to about 100 nm. *White arrow* points to lamelliform inclusion membrane, and *black arrowhead* points towards mitochondrion lying right next to the inclusion. *Bar* 1 µm. **b** 42 h p.i.: taking most of the space inside the host cell, the inclusion has grown to a size of 13 µm in diameter containing many different morphological forms of chlamydiae. Most of these organisms show a broadened periplasmic space (up to 400 nm) harbouring small membrane-bordered vesicles (50–100 nm). *White arrow* points to a smaller inclusion entirely coated by a complex of five directly opposing pairs of membranes (altogether 11 membranes). *N* host cell's nucleus, *bar* 2 µm, detail in *c*, *d*. **c**, **d** The *black arrowhead* points towards mitochondria outside the inclusion which do not show their typical christae, but seem to fall apart into small vesicles bordered by the outer mitochondrial membrane. *N* host cell's nucleus, *bar* 400 nm

widened at one pointed end giving just enough space to be tightly filled with vesicles. Due to the different duration of the developmental cycle (*C. trachomatis*: ~48 h, *C. pneumoniae*: ~72 h, *C. abortus*: ~56 h), the point of time of the occurrence of the vesicles varied between the species (Fig. 1). But the dynamic of the strict sequence of the occurrence of the different morphologies was the same in *C. trachomatis* and *C. pneumoniae* as it was in *C. abortus*.

All of these results were independent from the addition of cycloheximide and did not show any variance in McCoy cells compared to HeLa229 cells as host cells.

Discussion

In this study, we used electron microscopic methods to show several ultrastructural features of *C. abortus* amongst which the occurrence of vesicles in the periplasmic space of RBs in the late stage of the developmental cycle seems to be common with other chlamydial species, whereas the formation of massive membrane complexes inside the host cell is a *C. abortus* specific phenomenon.

Furthermore, projections and B-structures on the surface of *C. abortus* EBs were identified, which correspond

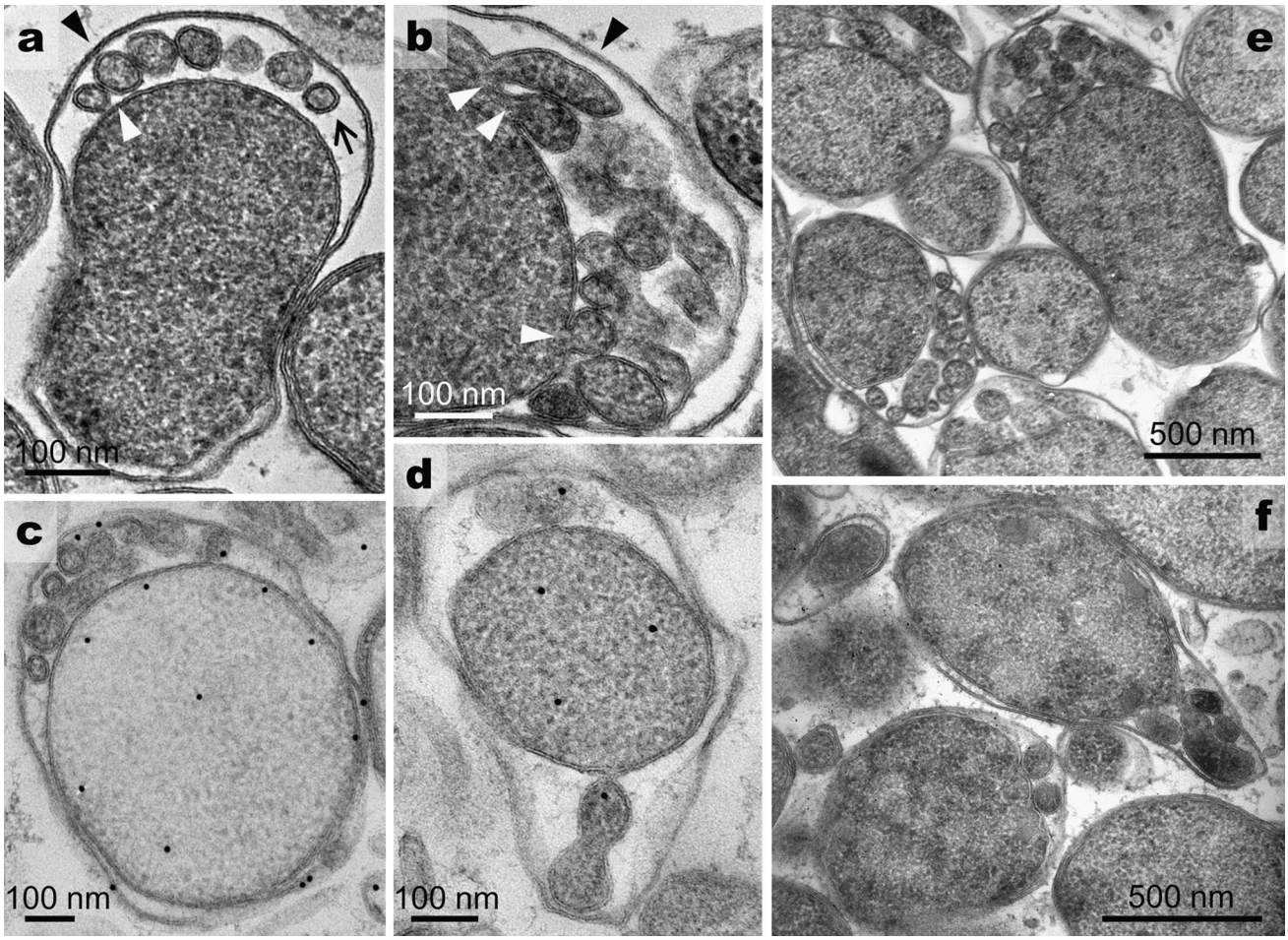

Fig. 8 RBs with vesicles in the periplasmic space of different species inside infected HeLa229 cells as seen by TEM: *C. abortus* (**a**, **b** 30 h p.i., **c**, **d** 42 h p.i., *bars* 100 nm), *C. trachomatis* (**e** 18 h p.i., *bar* 500 nm) and *C. pneumoniae* (**f** 40 h p.i., *bar* 500 nm). **a** *White and black arrowhead* point towards the inner and outer membrane of the RB; in between those membranes, there is the periplasmic space which harbours spherical membrane-bordered vesicles (*black arrow*) containing material showing the same electron density as the main body. These vesicles could be found in every infected host cell from 24 h p.i. to the late stages of the developmental cycle. **b** RB at another section level: the vesicles are still in connection with the main body, and they are possibly just budding off. **c**, **d** The immunogold-labelling of *C. abortus* RBs using a murine anti-chlamydial LPS-antibody (**c**) and a murine anti-chlamydial HSP60-antibody (**d**) with a goat antimouse-antibody coupled to 10 nm gold particles as secondary antibody indicates that the vesicles harbour chlamydial components. **e** *C. trachomatis* RBs show slightly smaller vesicles in the periplasmic space than *C. abortus* RBs on average. **f** *C. pneumoniae* RBs typically show an expansion of the periplasmic space at a pointed end of the RBs which harbours the vesicles

in detail to those structures first described by Matsumoto (1982b) and later hypothetically attributed to the T3SS of the *Chlamydiaceae* (Bavoil and Hsia 1998; Peters et al. 2007). The equipment of *C. abortus* with the T3SS seems to be probable since analysis of the genome revealed the presence of homologues to all genes thought to encode the chlamydial T3SS (Thomson et al. 2005). While a morphological as well as a molecular biological proof for the equipment with a functional T3SS apparatus has been provided for *C. trachomatis* (Gregory et al. 1979; Fields et al. 2003), *C. pneumoniae* (Miyashita et al. 1993; Lugert et al. 2004) and *C. psittaci* (Matsumoto 1973; Beeckman et al. 2008), the illustration of projections and B-structures on *C. abortus* EBs has been the first morphological evidence for the existence of the T3SS in *C. abortus*.

A phenomenon that seems to be exclusive to the species of *C. abortus* is the formation of membrane complexes that seem to develop from the inclusion membrane inside infected host cells at late stages of the developmental cycle. The questions we asked ourselves about the membrane complexes were: 'What material is used for their formation?' 'How are they formed?' and 'What function do they have?' At our momentary state of knowledge, answers to these questions are speculative. To gather material for the formation of such an amount of membranes, *C. abortus* would have to exploit the membrane pools of the host cell,

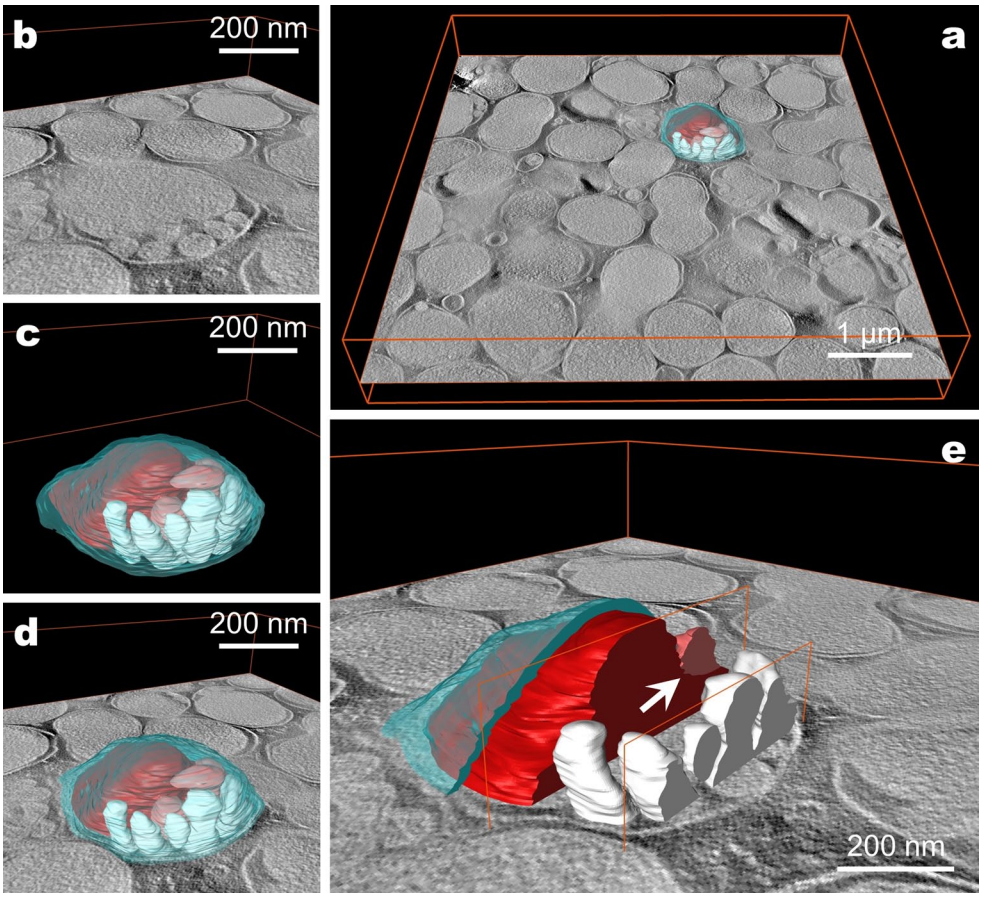

Fig. 9 Three-dimensional structure of *C. abortus* RB with vesicles in its periplasmic space inside an inclusion of an infected HeLa229 cell 30 h p.i. illustrated by STEM tomography and 3D reconstruction. **a** Overview, *bar* 1 µm. **b–e** The reconstructed RB consists of the main body (*red*): a homogenous, electron-dense mass with a size of about 700 nm in diameter bordered by a single membrane. The main body shows some protuberances (*light red*) that are possibly vesicles currently budding off (*white arrow*). Around the main body, there is another single membrane bordering the periplasmic space: the outer membrane of the RB (*transparent turquoise*). Besides the main body, there are further spherical and tubular bodies inside the periplasmic space (*white*) of the same electron density as the main body, but of smaller size of about 50–100 nm in diameter. *Bars* 200 nm

which are organelles such as the Golgi apparatus, the endoplasmatic reticulum and the mitochondria. Considering the close proximity to the inclusion, already described for *C. psittaci* by Matsumoto et al. (1991), and the seemingly perishing of mitochondria in the late stages of the developmental cycle, one might consider host mitochondria to be the origin of the membrane complexes of *C. abortus*. The ultrastructural similarity between the closely adjacent membranes of the membrane complexes and the inner and outer membrane of active mitochondria supports this idea (Höhn et al. 2011; Walther and Ziegler 2002).

Moreover, the question which chlamydial mechanisms are involved in the process of the membrane complex formation and material gathering is challenging. It is known that type three secreted virulence factors enable chlamydiae to hijack host cells' organelles (Heuer et al. 2009; Derré et al. 2011; Elwell et al. 2011). The family of Inc proteins found in all chlamydial species belongs to the type three secreted virulence factors (Dehoux et al. 2011). These proteins have been shown to be crucial for the formation and maintenance of the inclusion membrane (Lutter et al. 2012). A characteristic feature shared by all Inc proteins is a bilobal hydrophobic domain which is predicted to enable the Inc proteins' insertion into the inclusion membrane. Mital et al. (2013) recently showed that the ectopic expression of *C. trachomatis* Inc proteins with an intact bilobal hydrophobic domain in HeLa229 cells leads to the formation of 'membranous vesicular compartments'. The ultrastructure of these membranous vesicular compartments strongly reminds of the described membrane complexes of *C. abortus*. Therefore, Inc proteins might play an important role in the formation of the membrane complexes of *C. abortus*. *In silicio* predictions show that *C. abortus* is equipped with 72 putative Inc proteins (Dehoux et al. 2011). Further investigations on these Inc proteins may contribute to a better understanding of the formation of the observed membrane complexes.

However, the function behind these membrane complexes remains unclear. Because of the lack of a sufficient ribonucleoside triphosphates generation in chlamydiae and a permanent shortage of nutrients due to the living in an intracellular compartment (Saka and Valdivia 2010; Tipples and McClarty 1993; Stephens et al. 1998), the acquisition of such nutrients seems to be a probable suggestion. But as such membrane complexes could not be observed in other chlamydial species, the question emerges: is it imaginable that such an important mechanism is not conserved throughout the *Chlamydiaceae*?

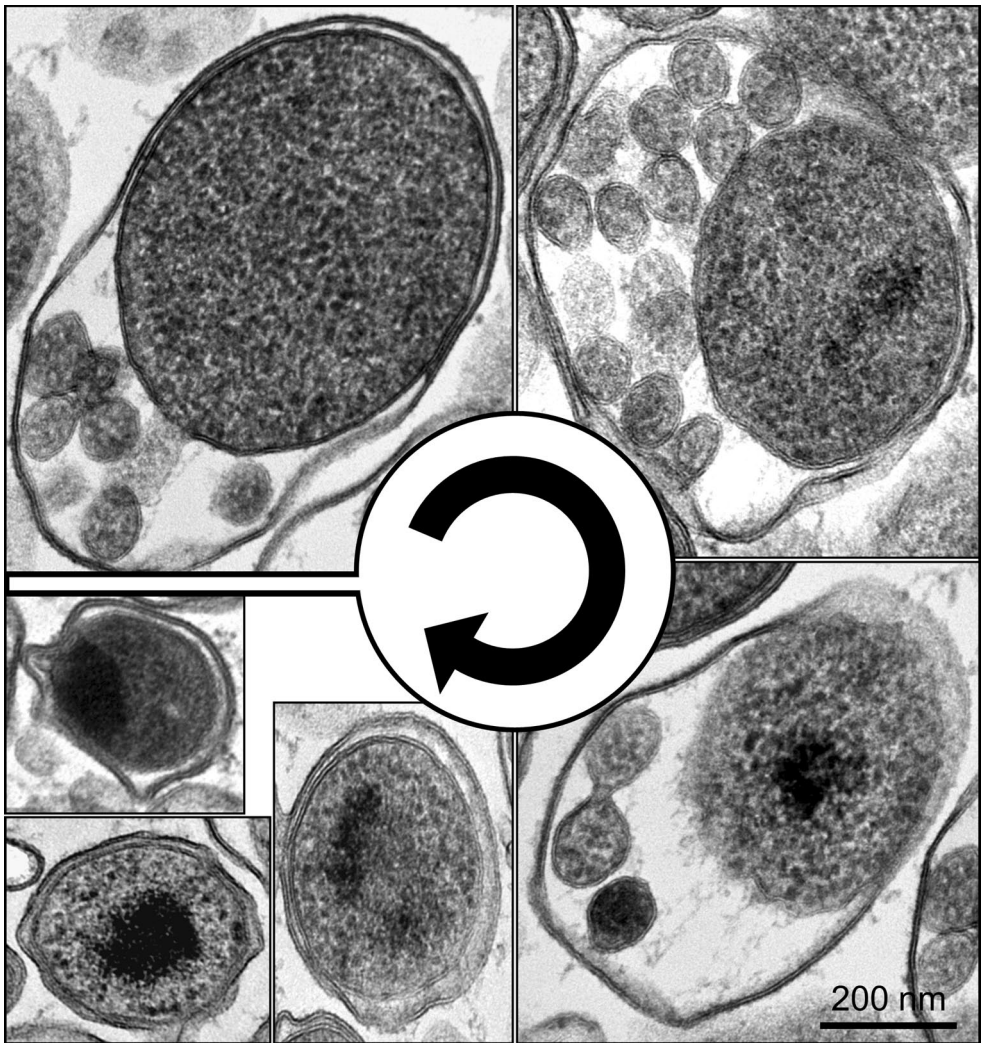

Fig. 10 A hypothetical composition of different *C. abortus* morphologies found inside HeLa229 cells 42/48 h p.i. as observed by TEM. The different morphologies may represent different stages of development. The *arrow* indicates a causal sequence of an RB redifferentiating into an EB at the end of the developmental cycle as a part of the condensation process. *Bar* 200 nm

The morphological appearance of the *Chlamydiaceae* can be classified into two distinct forms: EBs and RBs. In between those forms, there is the IB, a poorly defined form. We showed the existence of RBs with vesicles in the periplasmic space being an unknown morphological appearance of chlamydiae.

However, Tanami and Yamada (1973) described the formation of 'miniature cells' in *C. psittaci* looking quite the same as the RBs with vesicles in the periplasmic space mentioned here. Their explanation for the formation of miniature cells was a disturbance in membrane synthesis due to penicillin effects. Chi et al. (1987) described EBs of the TWAR strains of *C. pneumoniae* being enclosed by a wavy outer membrane and 'pear-shaped' in profile. In the widened periplasmic space, so-called 'miniature bodies [which] seemed to attach to the cytoplasmic mass by a thin peduncle' could be found. These ultra-structures also remind of the RBs with vesicles in the periplasmic space mentioned here. However, Kuo et al. (1988) did not find a penicillin dependent formation of these ultra-structures, but found out that the different morphology is linked to a function in the endocytosis of TWAR EBs by the host cell.

The occurrence of vesicles in the periplasmic space of RBs in the second half of the developmental cycle is independent of penicillin/cycloheximide addition, the type of host cells and type of chlamydial species. Therefore, we suggest that this ultrastructure is a common feature of *Chlamydiaceae* during their intracellular development. A likely function behind this distinct ultrastructure is the involvement in the redifferentiation process of RBs into EBs at the end of the developmental cycle. Little is known about the process of redifferentiation. Current conceptions

propose that every component of the RB, such as the genome, cytoplasm and membrane, is condensed forming the EB (Huang et al. 2010). We suggest that the ejection of vesicles might also play a role during the redifferentiation which is hypothetically illustrated in Fig. 10. The RB discards redundant material not needed in the metabolically inert EB by ejection of vesicles into the enlarged periplasmic space. This leads to a reduction in RB size. At the same time, DNA condensation takes place inducing the formation of the IB with its centric situated nucleus equivalent. Further condensation of the whole IB finally leads to the EB distinguished by its smaller size, its excentric situated nucleus equivalent and its cytoplasm with a higher electron density compared to RBs. Thus, the described morphology of RBs with vesicles in the periplasmic space is assigned a place in the process of re-differentiation as an intermediate step between the normally shaped RB and the IB. Clearly, further investigations are needed to elucidate the molecular functions behind the newly discovered ultra-structures of the *C. abortus* developmental cycle.

Acknowledgments We are grateful to Ulrike Simnacher and Corinna Foddis for expert technical help during cell culture and experimental infection. In addition, we would like to thank Eberhard Schmid and Renate Kunz for excellent technical assistance during sample processing for electron microscopy. This work was supported by the German Ministry for Education and Research (BMBF), 'Zoonotic chlamydiae—Models of chronic and persistent infections in humans and animals' Grant No. KI 0723, and by the German Research Foundation (DFG), SPP Grant No. 1580.

References

Baud D, Regan L, Greub G (2008) Emerging role of *Chlamydia* and *Chlamydia*-like organisms in adverse pregnancy outcomes. Curr Opin Infect Dis 21(1):70–76. doi:10.1097/QCO.0b013e3282f3e6a5

Bavoil PM, Hsia RC (1998) Type III secretion in *Chlamydia*: a case of déjà vu? Mol Microbiol 28(4):860–862

Bedson SP, Bland JOW (1932) A morphological study of psittacosis virus, with the description of a developmental cycle. J Exp Pathol 13:461–466

Beeckman DSA, Geens T, Timmermans J, van Oostveldt P, Vanrompay DCG (2008) Identification and characterization of a type III secretion system in *Chlamydophila psittaci*. Vet Res 39(3):27. doi:10.1051/vetres:2008002

Betts-Hampikian HJ, Fields KA (2010) The chlamydial type III secretion mechanism: revealing cracks in a tough nut. Front Microbiol 1:114. doi:10.3389/fmicb.2010.00114

Buser C, Walther P (2008) Freeze-substitution: the addition of water to polar solvents enhances the retention of structure and acts at temperatures around-60 degrees C. J Microsc 230(Pt 2):268–277. doi:10.1111/j.1365-2818.2008.01984.x

Chi EY, Kuo CC, Grayston JT (1987) Unique ultrastructure in the elementary body of *Chlamydia* sp. strain TWAR. J Bacteriol 169(8):3757–3763

Dehoux P, Flores R, Dauga C, Zhong G, Subtil A (2011) Multi-genome identification and characterization of chlamydiae-specific type III secretion substrates: the Inc proteins. BMC Genomics 12:109. doi:10.1186/1471-2164-12-109

Derré I, Swiss R, Agaisse H (2011) The lipid transfer protein CERT interacts with the *Chlamydia* inclusion protein IncD and participates to ER-*Chlamydia* inclusion membrane contact sites. PLoS Pathog 7(6):e1002092. doi:10.1371/journal.ppat.1002092

Elwell CA, Jiang S, Kim JH, Lee A, Wittmann T, Hanada K, Melancon P, Engel JN (2011) *Chlamydia trachomatis* co-opts GBF1 and CERT to acquire host sphingomyelin for distinct roles during intracellular development. PLoS Pathog 7(9):e1002198. doi:10.1371/journal.ppat.1002198

Fields KA, Mead DJ, Dooley CA, Hackstadt T (2003) *Chlamydia trachomatis* type III secretion: evidence for a functional apparatus during early-cycle development. Mol Microbiol 48(3):671–683

Fu Y, Baumann M, Kosma P, Brade L, Brade H (1992) A synthetic glycoconjugate representing the genus-specific epitope of chlamydial lipopolysaccharide exhibits the same specificity as its natural counterpart. Infect Immun 60(4):1314–1321

Gregory WW, Gardner M, Byrne GI, Moulder JW (1979) Arrays of hemispheric surface projections on *Chlamydia psittaci* and *Chlamydia trachomatis* observed by scanning electron microscopy. J Bacteriol 138(1):241–244

Heuer D, Rejman Lipinski A, Machuy N, Karlas A, Wehrens A, Siedler F, Brinkmann V, Meyer TF (2009) *Chlamydia* causes fragmentation of the Golgi compartment to ensure reproduction. Nature 457(7230):731–735. doi:10.1038/nature07578

Höhn K, Sailer M, Wang L, Lorenz M, Schneider ME, Walther P (2011) Preparation of cryofixed cells for improved 3D ultrastructure with scanning transmission electron tomography. Histochem Cell Biol 135(1):1–9. doi:10.1007/s00418-010-0765-z

Hsia RC, Pannekoek Y, Ingerowski E, Bavoil PM (1997) Type III secretion genes identify a putative virulence locus of *Chlamydia*. Mol Microbiol 25(2):351–359

Huang Z, Chen M, Li K, Dong X, Han J, Zhang Q (2010) Cryo-electron tomography of *Chlamydia trachomatis* gives a clue to the mechanism of outer membrane changes. J Electron Microsc (Tokyo) 59(3):237–241. doi:10.1093/jmicro/dfp057

Kremer JR, Mastronarde DN, McIntosh JR (1996) Computer visualization of three-dimensional image data using IMOD. J Struct Biol 116(1):71–76. doi:10.1006/jsbi.1996.0013

Kuo CC, Chi EY, Grayston JT (1988) Ultrastructural study of entry of *Chlamydia* strain TWAR into HeLa cells. Infect Immun 56(6):1668–1672

Longbottom D, Coulter LJ (2003) Animal chlamydioses and zoonotic implications. J Comp Pathol 128(4):217–244

Lugert R, Kuhns M, Polch T, Gross U (2004) Expression and localization of type III secretion-related proteins of *Chlamydia pneumoniae*. Med Microbiol Immunol 193(4):163–171. doi:10.1007/s00430-003-0206-x

Lutter EI, Martens C, Hackstadt T (2012) Evolution and conservation of predicted inclusion membrane proteins in chlamydiae. Comp Funct Genomics 2012:362104. doi:10.1155/2012/362104

Matsumoto A (1973) Fine structures of cell envelopes of *Chlamydia* organisms as revealed by freeze-etching and negative staining techniques. J Bacteriol 116(3):1355–1363

Matsumoto A (1982a) Electron microscopic observations of surface projections on *Chlamydia psittaci* reticulate bodies. J Bacteriol 150(1):358–364

Matsumoto A (1982b) Surface projections of *Chlamydia psittaci* elementary bodies as revealed by freeze-deep-etching. J Bacteriol 151(2):1040–1042

Matsumoto A, Manire GP (1970) Electron microscopic observations on the fine structure of cell walls of *Chlamydia psittaci*. J Bacteriol 104(3):1332–1337

Matsumoto A, Bessho H, Uehira K, Suda T (1991) Morphological studies of the association of mitochondria with chlamydial inclusions and the fusion of chlamydial inclusions. J Electron Microsc (Tokyo) 40(5):356–363

Mital J, Miller NJ, Dorward DW, Dooley CA, Hackstadt T (2013) Role for chlamydial inclusion membrane proteins in inclusion membrane structure and biogenesis. PLoS One 8(5):e63426. doi:10.1371/journal.pone.0063426

Miyashita N, Kanamoto Y, Matsumoto A (1993) The morphology of *Chlamydia pneumoniae*. J Med Microbiol 38(6):418–425

Peters J, Wilson DP, Myers G, Timms P, Bavoil PM (2007) Type III secretion à la *Chlamydia*. Trends Microbiol 15(6):241–251. doi:10.1016/j.tim.2007.04.005

Roth J, Zuber C, Komminoth P, Sata T, Li WP, Heitz PU (1996) Applications of immunogold and lectin-gold labeling in tumor research and diagnosis. Histochem Cell Biol 106(1):131–148

Saka HA, Valdivia RH (2010) Acquisition of nutrients by Chlamydiae: unique challenges of living in an intracellular compartment. Curr Opin Microbiol 13(1):4–10. doi:10.1016/j.mib.2009.11.002

Stephens RS, Kalman S, Lammel C, Fan J, Marathe R, Aravind L, Mitchell W, Olinger L, Tatusov RL, Zhao Q, Koonin EV, Davis RW (1998) Genome sequence of an obligate intracellular pathogen of humans: *Chlamydia trachomatis*. Science 282(5389):754–759

Studer D, Michel M, Müller M (1989) High pressure freezing comes of age. Scanning Microsc Suppl 3:253–268 discussion 268–269

Tanami Y, Yamada Y (1973) Miniature cell formation in *Chlamydia psittaci*. J Bacteriol 114(1):408–412

Thomson NR, Yeats C, Bell K, Holden MTG, Bentley SD, Livingstone M, Cerdeño-Tárraga AM, Harris B, Doggett J, Ormond D, Mungall K, Clarke K, Feltwell T, Hance Z, Sanders M, Quail MA, Price C, Barrell BG, Parkhill J, Longbottom D (2005) The *Chlamydophila abortus* genome sequence reveals an array of variable proteins that contribute to interspecies variation. Genome Res 15(5):629–640. doi:10.1101/gr.3684805

Tipples G, McClarty G (1993) The obligate intracellular bacterium *Chlamydia trachomatis* is auxotrophic for three of the four ribonucleoside triphosphates. Mol Microbiol 8(6):1105–1114

Walder G, Hotzel H, Brezinka C, Gritsch W, Tauber R, Würzner R, Ploner F (2005) An unusual cause of sepsis during pregnancy: recognizing infection with *chlamydophila abortus*. Obstet Gynecol 106(5 Pt 2):1215–1217. doi:10.1097/01.AOG.0000161060.69470.9c

Walther P (2003) Recent progress in freeze-fracturing of high-pressure frozen samples. J Microsc 212(Pt 1):34–43

Walther P, Ziegler A (2002) Freeze substitution of high-pressure frozen samples: the visibility of biological membranes is improved when the substitution medium contains water. J Microsc 208(Pt 1):3–10

Walther P, Wehrli E, Hermann R, Müller M (1995) Double-layer coating for high-resolution low-temperature scanning electron microscopy. J Microsc 179(Pt 3):229–237

Walther P, Schmid E, Höhn K (2013) High-pressure freezing for scanning transmission electron tomography analysis of cellular organelles. Methods Mol Biol 931:525–535. doi:10.1007/978-1-62703-056-4_28